C. R. Mecanique 346 (2018) 701–711

Contents lists available at ScienceDirect

Comptes Rendus Mecanique

www.sciencedirect.com

Computational modeling of material forming processes / Simulation numérique des procédés de mise en forme

3D numerical simulation of drilling residual stresses

Mathieu Girinon [a], Frédéric Valiorgue [b], Habib Karaouni [c], Éric Feulvarch [b,*]

[a] CETIM, 52, avenue Félix-Louat, 60300 Senlis, France
[b] Univ. Lyon, ENISE, LTDS, UMR 5513 CNRS, 58, rue Jean-Parot, 42023 Saint-Étienne cedex 2, France
[c] SAFRAN Tech, rue des Jeunes-Bois, 78772 Magny-les-Hameaux, France

ARTICLE INFO

Article history:
Received 27 October 2017
Accepted 21 December 2017
Available online 15 June 2018

Keywords:
Drilling processes
Residual stresses
Numerical simulation

ABSTRACT

Drilling can affect the integrity of the surface of a mechanical component and reduce its fatigue life. Thus, drilling parameters such as lubrication or drilling velocity must be optimized to ensure a satisfactory residual mechanical state of the hole surfaces. Unfortunately, experimental tests are time consuming and it is not easy to observe the cutting process because of the confinement of the drill zone. The literature does not exhibit any numerical simulation capable of simulating 3D thermomechanical phenomena in the drill zone for large depth holes. Therefore, residual stresses cannot be easily simulated by means of the sole drilling parameters. The aim of this article is to propose a new numerical approach to compute drilling residual stresses for large-depth holes. A first simulation is developed to simulate heat transfer by means of a 3D thermoviscoplastic simulation in a new Rigid-ALE framework allowing the use of large calculation time steps. Then, a time interpolation and a spatial projection are implemented to rebuild the Lagrangian thermal history of the machined component. Finally, a thermo-elastoplastic simulation is carried out to compute residual stresses in the final workpiece. In this paper, the method is applied to a 316L austenitic stainless steel in the case of an unlubricated hole. The computed residual stresses are compared to experimental measurements.

1. Introduction

During the manufacturing of aeronautical, nuclear or medical parts, drilling processes are often used to perform holes. All the machining processes impose thermal and mechanical loadings on the machined part, which modifies the surface integrity and thus, the fatigue lifetime. Compared to other processes such as turning or milling, the experimental study of drilling is difficult because of the confinement of the drill zone. To avoid such an issue, numerical simulation is of particular interest, since it allows studying the local thermomechanical phenomena in 3D.

Different types of numerical models are developed in the literature for drilling processes. The less predictive models use temperature measurements to estimate thermal loadings, as proposed by Huang et al. [1] and Sousa et al. [2]. These models do not consider the mechanical coupling in the heat generation process, but they can provide thermal input data to study phase transformations as proposed by Schulze et al. [3]. Wu and Han [4] developed a numerical model in 2D by means of various finite element codes. They studied the cutting area near the center of the drill zone and in the main cutting

* Corresponding author.
E-mail address: eric.feulvarch@enise.fr (É. Feulvarch).

https://doi.org/10.1016/j.crme.2018.06.003

zone in planes perpendicular to the cutting edge to determine where the temperature is highest. Ozcelik and Bagci [5] also used a 2D numerical approach to study the cutting phenomena along the cutting zone, and they compared results for two materials: AISI 1040 and Al 7075-T651. This 2D approach is unable to give the 3D thermomechanical loadings required for studying the surface integrity of the final holes.

Most of the existing 3D numerical models in drilling processes pose challenges to simulate the machining of a significant drilling depth. Nan et al. [6] simulate a drilling time of about 0.03 s by means of Abaqus/Explicit. Abouridouane et al. performed several studies on the thrust force, the torque and the chip geometry for micro-drilling with Deform-3D [7][8][9]. They also studied a classical drilling configuration with a drill diameter of 8 mm [10] and the simulated time was about 80 ms, which corresponds to a small depth. A similar configuration was studied by Marusich et al. [11] with the code Third Wave Advantedge, whereas Muhamad et al. used MSC Marc [12] and Deform-3D [13]. To simulate the removal of the material, these numerical models are based on an explicit time integration leading to a very high computation time. Moreover, they use a Lagrangian description for the material movement description. Therefore, the computing time is increased because of the need for successive remeshing operations to avoid mesh distortions. Thus, the drilling time simulated is always low and only thrust force, torque and chip geometry can be compared with the experimental data.

The literature does not exhibit any numerical simulation capable of simulating 3D thermomechanical phenomena in the drill zone for very deep holes. In turning processes, Valiorgue et al. [14] avoid the simulation difficulties of the chip generation by replacing the physical effects of the cutting zone by an equivalent thermomechanical loading applied on the final surface after machining. This loading is built intuitively from experimental measurements. To avoid such an intuitive stage, a new numerical approach is proposed in section 2 of this paper to compute drilling residual stresses for holes of large depths. In section 3, a first simulation is developed to simulate heat transfer by means of a 3D thermoviscoplastic simulation in a new Rigid-ALE framework. In section 4, a time interpolation and a spatial projection are implemented to rebuild the Lagrangian thermal history of the machined component. Thus, a thermo-elastoplastic simulation can be carried out to compute residual stresses on the final geometry. The whole method is applied to an 316L austenitic stainless steel in the case of an unlubricated hole. The computed residual stresses are compared to experimental measurements.

2. A new numerical strategy

From the computational point of view, the main difficulty lies in the simulation of chip generation. Indeed, this needs the use of a damage model, difficult to calibrate because of the material's elasticity, which prevents the separation of the chips from the rest of the material. Moreover, elasticity imposes to track the material flow and this can lead to mesh distortions requiring remeshing steps and projections of results from one mesh to another. In 3D, such an approach is very CPU time consuming. Unfortunately, the computation of drilling residual stresses needs to take account of the elasticity. In this work, we propose to compute residual stresses by means of a step-by-step method that is composed of two successive simulations, as shown in Fig. 1.

The objective of the first one is to simulate the thermomechanical effects due to the removal of the material by means of the drilling process parameters. This thermomechanical simulation is based on a viscoplastic behavior law avoiding elasticity and, therefore, on the use of a damage model. As far as the mesh is concerned, a new Rigid-ALE technique is proposed to avoid mesh distortion. The method R–ALE combines the Lagrangian, Eulerian, and ALE characteristics according to the part of the model considered. A part of the mesh can move between two successive configurations without distortions by means of rigid movements. Because we do not consider elasticity, hardening, and damage, there is no need to project the results from one mesh to another. The material time derivatives are classically treated by means of the standard ALE technique, which consists in defining a convection velocity relatively to the mesh movement. To reduce the computing time, a backward Euler algorithm tolerating relatively large time steps is adopted for time integration. After the R–ALE simulation, a transfer step is carried out for rebuilding the Lagrangian history of the final workpiece in terms of temperatures in the case of an unlubrificated drill. Thus, a Lagrangian thermo-elastoplastic computation can easily be carried out for computing residual stresses.

3. Thermo-mechanical R–ALE simulation of the drilling process

3.1. Physical modeling

3.1.1. Material flow

Assuming that viscous stresses are predominant, the momentum balance is governed by the following equation:

$$\mathbf{div}(\boldsymbol{\sigma}) = \mathbf{0} \tag{1}$$

$\boldsymbol{\sigma}$ denotes the Cauchy stress tensor:

$$\boldsymbol{\sigma} = \mathbf{S} - \mathrm{p} \cdot \mathbf{I}$$

where p is the hydrostatic pressure, $\mathbf{I}$ is the unit second-order tensor and $\mathbf{S}$ is the deviatoric stress tensor. As for hot forming processes, a viscous behavior law is used to model the material flow in the cutting area. This law can be represented as follows:

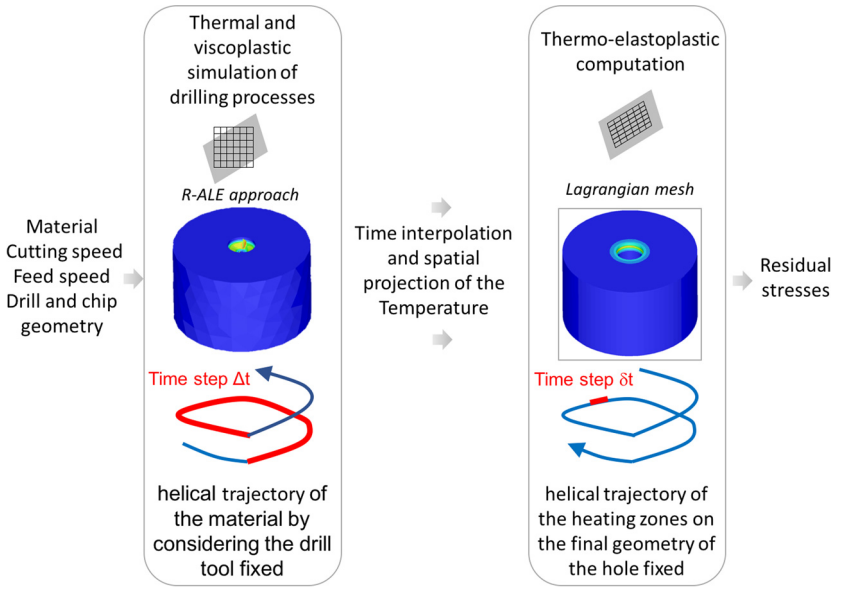

Fig. 1. The new strategy for the computation of drilling residual stresses.

$$\mathbf{S} = 2\,\mu\,\mathbf{D}^{\mathrm{vp}} \tag{2}$$

where μ is the dynamic viscosity and $\mathbf{D}^{\mathrm{vp}}$ is the viscoplastic strain rate tensor. Assuming the additive decomposition of the strain rate and considering the predominance of the viscoplastic strain rate in the drill zone, we get:

$$\mathbf{D}^{\mathrm{vp}} = \mathbf{D} - \mathbf{D}^{\mathrm{e}} - \mathbf{D}^{\mathrm{th}} \approx \mathbf{D} = \frac{1}{2}\left(\mathbf{grad}^{t}(\mathbf{v}) + \mathbf{grad}(\mathbf{v})\right)$$

where $\mathbf{D}^{\mathrm{e}}$ and $\mathbf{D}^{\mathrm{th}}$ denote respectively the elastic strain rate tensor and the thermal strain rate tensor; $\mathbf{v}$ is the material velocity of the material.

The momentum balance equation (1), combined with the constitutive equation (2), thus leads to:

$$\mathbf{div}(2\,\mu\,\mathbf{D}) - \mathbf{grad}\,\mathrm{p} = \mathbf{0} \tag{3}$$

To ensure the viscoplastic incompressibility, the velocity field must be divergence free:

$$\mathbf{div}(\mathbf{v}) = 0 \tag{4}$$

Eqs. (3) and (4) are only solved in the chips by means of the finite element $P1+/P1$ (Fig. 2) that is very common for modeling hot forming processes [15]. For this tetrahedral element, the discrete field of pressure p^{h} is linear and continuous. Index '+' means that a node has been added for the interpolation of velocity $\mathbf{v}^{\mathrm{H}}$ ($P1+$), so that:

$$\mathbf{v}^{\mathrm{H}} = \mathbf{v}^{\mathrm{h}} \oplus \mathbf{v}^{\mathrm{b}}$$

where $\mathbf{v}^{\mathrm{h}}$ represents the linear part ($P1$) and $\mathbf{v}^{\mathrm{b}}$, the bubble part of the velocity field. $\mathbf{v}^{\mathrm{H}}$ is of the form

$$\mathbf{v}^{\mathrm{H}} = \sum_{i=1}^{N} \mathbf{v}_i^{h}\, N_i + \sum_{j=1}^{M} \mathbf{v}_j^{\mathrm{b}}\, N_j^{\mathrm{b}} \tag{5}$$

In this expression, N denotes the number of nodes and M denotes the number of elements, $\mathbf{v}_i^{\mathrm{h}}$ the value of the velocity at node i and N_i the shape function associated with this node. $\mathbf{v}_j^{\mathrm{b}}$ is the velocity value at each internal node located at the center of each element and N_i^{b} denotes the associated shape function which is equal to zero on the element boundaries. The chosen interpolation function corresponds to the h-refining type, *i.e.* it is of degree 1 piecewise inside the tetrahedron.

3.1.2. Heat transfer

Dissipation due to the generation of chips causes a temperature rise in the macroscopic scaling. Heat transfers are governed by the following equation:

$$\rho C\left(\frac{\partial\theta}{\partial t} + \mathbf{v}_{\mathrm{cv}}\,\mathbf{grad}\,\theta\right) = \mathrm{div}\,(\lambda\,\mathbf{grad}\,\theta) + Q \tag{6}$$

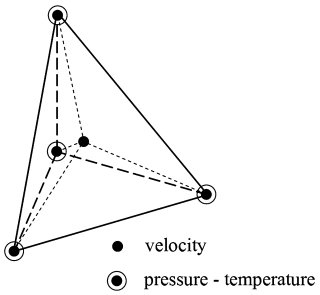

Fig. 2. Reference P1+/P1 tetrahedron.

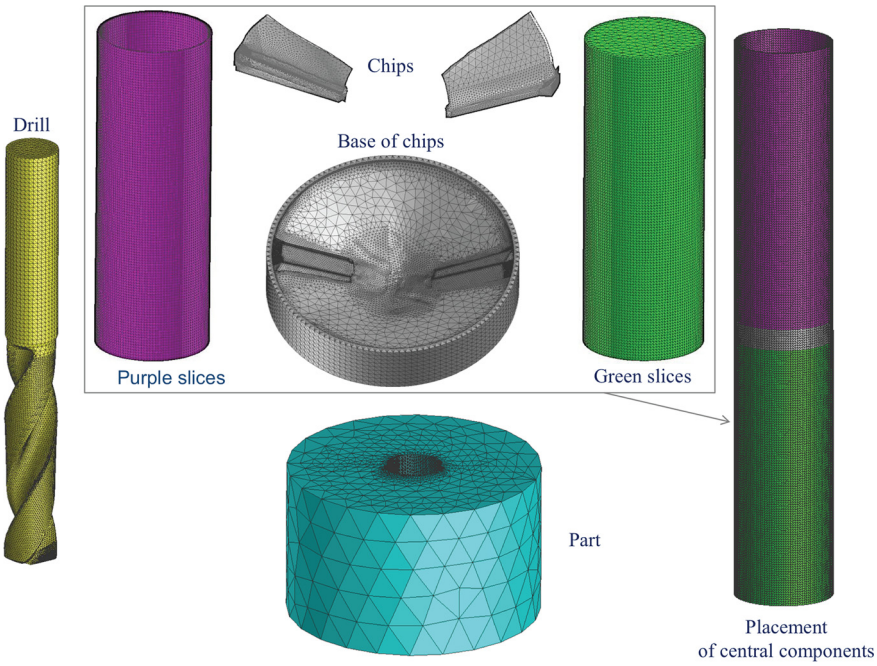

Fig. 3. Partitions of the mesh for R–ALE.

In this equation solved in the whole model including the drill tool, λ is thermal conductivity, which can be temperature dependent; ρ is mass density; C is specific heat; θ is temperature and $\mathbf{v}_{cv}$ is convective velocity. During the drilling processes, heat transfer is fast both for heating and cooling. It is partly caused by the mechanical power derived from the material flow in the cutting zone:

$$Q = \alpha\, \mathbf{S} : \mathbf{D}$$

where α is the Taylor–Quinney coefficient, which is less than 1 when the mechanical power does not entirely dissipate in the form of heat.

With regard to boundary conditions, the heat exchange with the external media is modeled by means of an exchange coefficient h_{ext}:

$$q = h_{ext}\,(\theta^{ext} - \theta) \tag{7}$$

where θ^{ext} denotes the temperature of the external media and q is the density of the heat flux received by the workpiece or the drill tool.

3.2. The R–ALE kinematic

The different parts of the mesh used by the R–ALE method are presented in Fig. 3. The green part represents the geometry before the drilling stage and the purple part includes the geometry of the complete hole after drilling. The mesh parts are created by means of CAD software. As proposed by Girinon et al. [16] for the simulation of turning, the geometry of chips is the result of Quick Stop Drilling tests (QSD) assuming that it does not change significantly during all

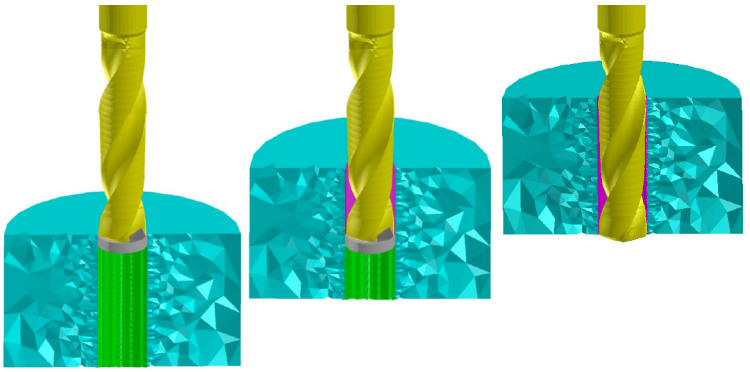

Fig. 4. Schematic representation of the R–ALE kinematic.

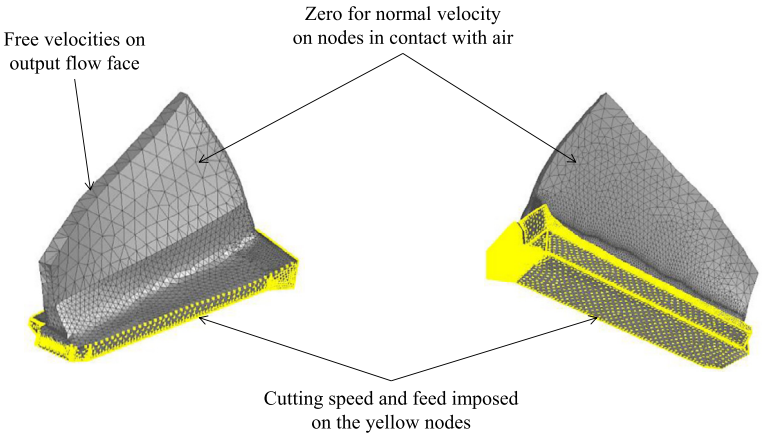

Fig. 5. Mechanical boundary conditions for the chips.

the drilling stage. This experimental set-up has been developed by Claudin [17]. It consists in stopping instantaneously a drilling operation and then, in scanning the geometry of the chips for building a 3D CAD model. All the parts are easily meshed by means of linear tetrahedral elements.

The whole mesh is considered as being rigid, and thus, the mesh of the chips is not deformable during all the simulation. The Lagrangian mesh of the drill is fixed. This means that the reference frame is not the classical fixed one associated with the workpiece; it rotates with the drill so that the drill remains fixed in space. In the blue Eulerian part of the workpiece, the material has a rotational velocity, whereas the mesh just goes up at each computing time step Δt, which corresponds to one advance per revolution. This means that the height of the finite elements depends on the cutting velocity for obtaining a conformal mesh at each time step, as proposed by Feulvarch et al. [18] for the rotation of a FSW tool. In this way, the material has a helical trajectory and the number of computing time steps is equal to the number of revolutions needed to create the hole. In practice, the computing time step can be twice or three times greater if the advance per revolution is relatively small. At each time step, the green and purple finite elements that do not belong to the actual geometry of the workpiece are not considered for the computation (see Fig. 4).

In order to reduce the computing time, the mechanical calculation is only carried out in the chips, whereas the velocity is imposed in the other parts. On the base of the chips, the green and purple parts, a vertical component of velocity is added compared to the blue part to model the upward movement of the material. The same velocity field is imposed at the interface between the chips and the base of the chips, as shown in Fig. 5. A zero normal velocity is prescribed on the free surfaces to ensure that the material flow follows well the geometry of the chips obtained experimentally.

In each part of the mesh, the convective velocity is classically defined as follows:

$$\mathbf{v}_{\text{cv}} = \mathbf{v} - \mathbf{v}_{\text{mesh}} \tag{8}$$

where $\mathbf{v}_{\text{mesh}}$ denotes the velocity of the mesh. An implicit (backward) Euler algorithm tolerating relatively large time steps is adopted by evaluating the time derivative of the temperature at time $t + \Delta t$ as follows:

$$\frac{\partial \theta}{\partial t}(t + \Delta t) \approx \frac{\theta_{t+\Delta t} - \theta_t}{\Delta t}$$

Table 1
Thermal properties of 316L stainless steel (workpiece).

θ	ρ (kg/m^3)	C (J/kg/°C)	λ (W/m/°C)
20 °C	8000	450	14
100 °C	7970	490	15.2
200 °C	7940	525	16.6
300 °C	7890	545	17.9
400 °C	7850	560	19
500 °C	7800	570	20.6
600 °C	7750	580	21.8
700 °C	7700	595	23.1
800 °C	7660	625	24.3
900 °C	7610	650	26
1000 °C	7570	660	27.3
1200 °C	7450	677	29.9

Table 2
Thermal properties of tungsten carbide (drill tool).

θ	ρ (Kg/m^3)	C (J/kg/°C)	λ (W/m/°C)
20 °C	14830	220	110
100 °C	14830	244	105
300 °C	14830	290	98
500 °C	14830	320	90
700 °C	14830	328	82
900 °C	14830	337	75
1100 °C	14830	338	66

3.3. Application to the drilling of a 316L stainless steel

The numerical methodology presented above is applied to a 316L drilling operation. The simulation has been performed using the computer code Sysweld® [19]. The drilling conditions are:

- cutting velocity, 60 m/min,
- feed, 0.15 mm/rev,
- drill diameter, 12 mm,
- drilled length, 36 mm,
- through-hole,
- dry drilling,
- workpiece diameter, 60 mm.

In this application, the Taylor–Quinney coefficient α is taken equal to 0.9, as proposed by Zaera et al. [20]. The thermal contact is assumed to be perfect between the drill tool and the workpiece. As far as the thermal boundary conditions are concerned (see Eq. (7)), θ^{ext} and h_{ext} are defined by considering:

- convection on the surfaces located outside the hole, exchange coefficient: 40 $\text{W} \cdot \text{m}^{-2} \cdot {}^\circ\text{C}^{-1}$, room temperature: 20 °C.
- convection in the drilled hole, exchange coefficient: 50 $\text{W} \cdot \text{m}^{-2} \cdot {}^\circ\text{C}^{-1}$, room temperature: 100 °C.

The thermal properties of the workpiece and of the drilling tool are respectively given in Tables 1 and 2.

The temperature-dependent viscosity of the material has been identified by means of the Lurdos law established for the 304L stainless steel [21]. This law is an empirical model based on the classical Voce equation. The high temperatures and the high strain rates are considered to give an accurate representation of the phenomena in the primary shearing area, which are assumed to be the main heating phenomena in this unlubricated case study. As shown in Fig. 6, the maximal temperature in the cutting area is about 900°C, whereas the temperature is about 500°C on the surface of the hole near the drill zone.

Fig. 7 shows the comparison between the thermal kinetics computed at mid-depth and two experimental measurements obtained with thermocouples located 1.3 mm ahead from the final surface in the blue part (see Fig. 3). One can note that the temperature peaks are close to each other and that the cooling stage is well simulated. The new R–ALE method leads to a CPU time of about 20 h with tetrahedron finite elements of type P1+/P1 [18].

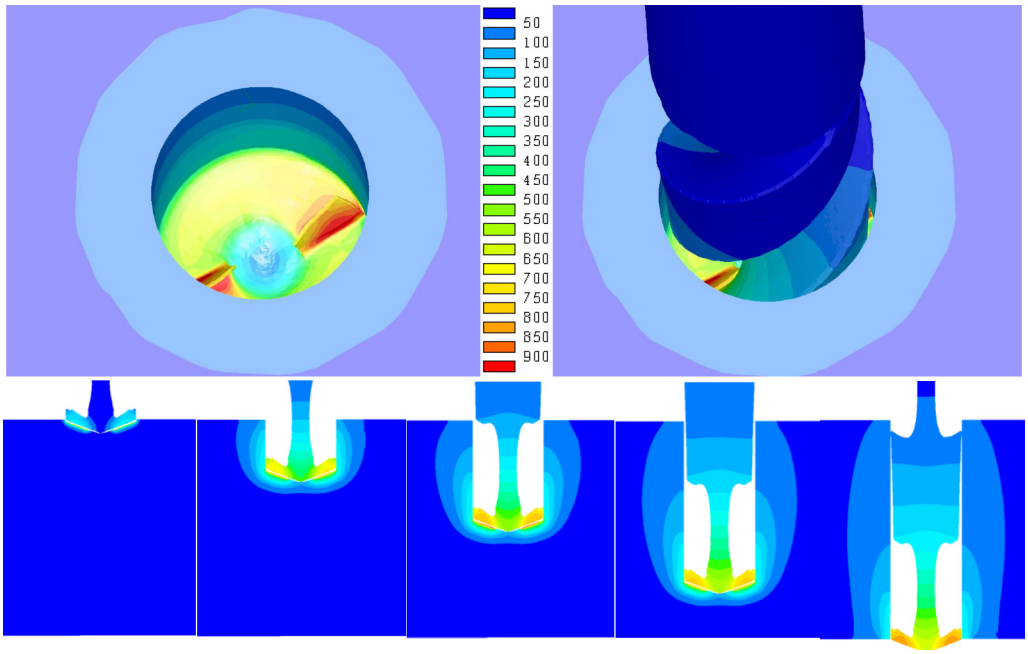

Fig. 6. Distribution of temperature (°C) during drilling.

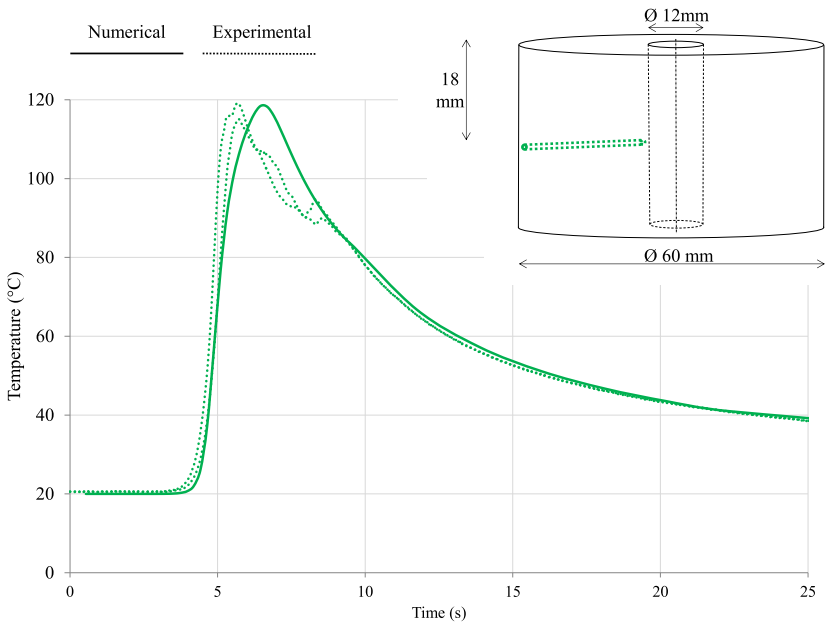

Fig. 7. Numerical and experimental thermal kinetics at mid-depth during drilling.

4. Computation of drilling residual stresses

4.1. Rebuilding the Lagrangian thermal history from R–ALE results

Considering the case of an unlubricated drilling process, the traction residual stresses on the surface of the holes are mainly due to thermal loadings, as shown by Girinon et al. [22]. In the numerical approach proposed in this work, the computation of residual stresses is simulated in a Lagrangian approach because the integration of the material history is simple and quick to compute in such a configuration. The simulation is then carried out on a Lagrangian mesh that corresponds to the final geometry of the hole. Unfortunately, the R–ALE does not give directly the material history of the machined component in a Lagrangian way, as explained in the above section. Moreover, the thermal results are obtained

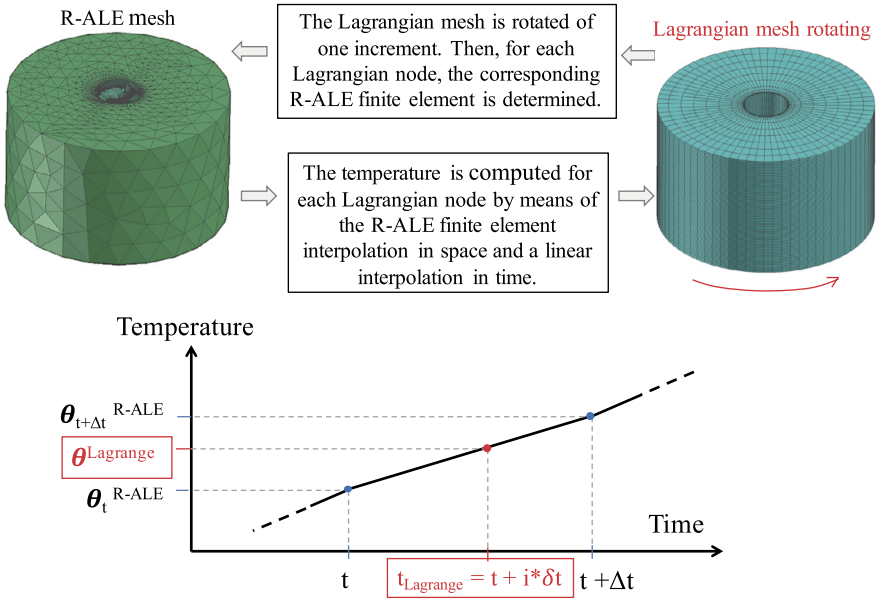

Fig. 8. Schematic representation of the projection technique implemented for rebuilding the Lagrangian thermal history.

with a time step Δt corresponding to a rotation of the drill tool. This time step leads to a satisfactory computational precision, but it is too large to track accurately the thermal history at each point of the machined surface. Therefore, a time interpolation and a spatial projection need to be implemented to rebuild the Lagrangian thermal history.

It consists in prescribing a vertical translation to the Lagrangian mesh like that of the blue Eulerian part in the R–ALE simulation (see Fig. 4), but also a rotation to follow the material movement of the workpiece by always considered the drill tool fixed. A sub time step δt is defined for the projection as follows:

$$\delta t = \frac{\Delta t}{n}$$

where n is the number of angular positions during one rotation of the Lagrangian mesh. At each projection time, each node of the Lagrangian mesh is projected onto the corresponding R–ALE mesh configuration and its temperature is computed by means of the finite element approximation in space and of the linear interpolation in time, as shown in Fig. 8.

4.2. Computation of residual stresses

The residual stress analysis is based on the momentum balance equation given by

$$\mathbf{div}\,\boldsymbol{\sigma} = \mathbf{0} \tag{9}$$

It is performed with the infinitesimal strain theory. Therefore, $\boldsymbol{\sigma}$ is assumed to depend linearly on the elastic strain tensor $\boldsymbol{\epsilon}^e$ by means of the fourth-rank elastic tensor $\mathbf{C}$ as follows

$$\boldsymbol{\sigma} = \mathbf{C} : \boldsymbol{\epsilon}^e \tag{10}$$

As the effect of plastic dissipation on heat transfer is neglected in the material included in the final Lagrangian geometry after drilling, heat transfers coming from the R–ALE simulation are mainly involved in the mechanical analysis through the thermal strains [23]. The strain rate tensor $\mathbf{D}$ is thus decomposed into a thermal part $\mathbf{D}^{\mathrm{th}}(\theta)$, an elastic part $\mathbf{D}^{\mathrm{e}}$ and a plastic part $\mathbf{D}^{\mathrm{p}}$:

$$\mathbf{D} = \mathbf{D}^{\mathrm{th}}(\theta) + \mathbf{D}^{\mathrm{e}} + \mathbf{D}^{\mathrm{p}} \tag{11}$$

4.3. Application to the computation of residual stresses in a 316L steel

After rebuilding, the Lagrangian temperature distribution is plotted in Fig. 9 at mid-depth on the Lagrangian mesh of the hole made of linear hexahedron finite elements.

In Fig. 9, one can note that the mesh is refined in a zone of interest so as to have a better estimation of residual stresses in this area without increasing the computing time too much. Residual stresses are computed by means of a model

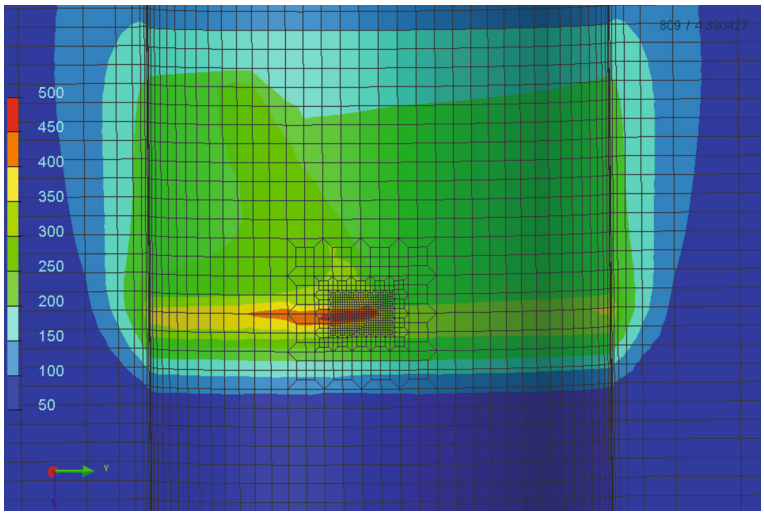

Fig. 9. Distribution of the Lagrangian temperature (°C) at mid-depth of the hole.

Table 3
Thermo-elastic properties of 316L stainless steel.

θ	20 °C	200 °C	400 °C	600 °C	800 °C
E (MPa)	201 730	194 220	181 770	166 860	144 000
Thermal expansion	$1.22{\cdot}10^{-5}$	$1.32{\cdot}10^{-5}$	$1.4{\cdot}10^{-5}$	$1.45{\cdot}10^{-5}$	$1.62{\cdot}10^{-5}$
σ^y (MPa)	530	440	364	294	229
$\epsilon^p = 0.01$	580	482	398	322	251
$\epsilon^p = 0.02$	609	506	418	339	264
$\epsilon^p = 0.03$	634	527	435	352	274
$\epsilon^p = 0.04$	655	545	450	364	284
$\epsilon^p = 0.05$	676	561	464	376	292
$\epsilon^p = 0.1$	761	632	522	423	329
$\epsilon^p = 0.2$	895	744	615	498	388
$\epsilon^p = 0.3$	1008	838	693	561	436
c	$7.5{\cdot}10^4$	$6.6{\cdot}10^4$	$5.6{\cdot}10^4$	$6.5{\cdot}10^4$	$8{\cdot}10^4$
γ	300	290	280	350	1000

of the 'Armstrong–Frederick' type [24] to take into account the cyclic elastoplastic behavior due to the successive thermal sollicitations induced by the rotation of the drill tool. This law considers an isotropic and a non-linear kinematic hardening defined by:

$$\dot{\boldsymbol{\chi}} = \frac{2}{3} c\, \mathbf{D}^p - \gamma\, \boldsymbol{\chi}\, D^p$$

where $\dot{\boldsymbol{\chi}}$ denotes the time derivative of the kinematic variable $\boldsymbol{\chi}$; D^p is the equivalent plastic strain rate; c and γ are two parameters given in Table 3. In this application, the Poisson coefficient is taken equal to 0.3.

The residual stresses are observed in the refined part of the Lagrangian mesh (see Fig. 9). The experimental and numerical distributions of residual stresses at mid-depth of the hole are plotted in Fig. 10 as a function of the distance from the surface. The experimental residual stresses are plotted with an envelope curve to show the experimental dispersion obtained with three samples. The CPU time for the computation of residual stresses is about 30 h.

One can note that the simulation leads to traction residual stresses along the circumferential and axial directions. Moreover, the circumferential stress is the highest one observed experimentally. The comparison of experimental and numerical residual stresses on the surface is satisfactory even if a significant difference can be observed in the volume of material under the surface. This can be due to the thermomechanical contact between the drill tool and the surface of the hole, which is not yet integrated in the numerical model developed.

5. Conclusion

A new numerical strategy is proposed in this article to compute drilling residual stresses. A new R–ALE technique allows simulating a complete drilling operation by considering a viscoplastic flow in the chips. This simulation uses a computing

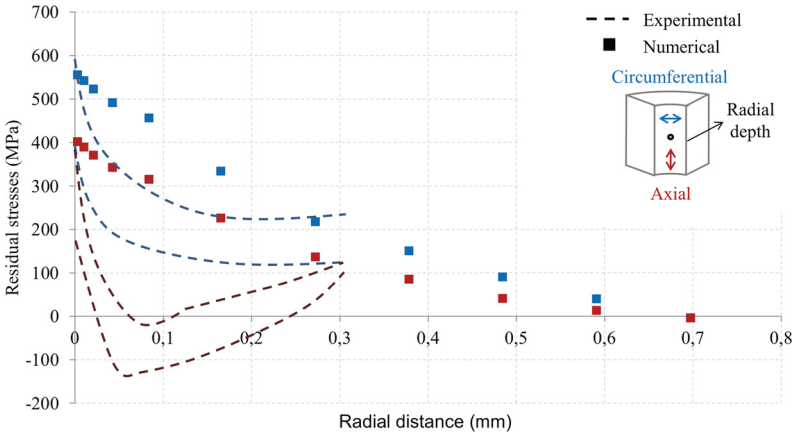

Fig. 10. Distribution of residual stresses at mid-depth of the hole.

time step equal to a rotation of the drilling tool and it does not induce mesh distortions. Therefore, the computing time is reduced because it is a few hours. A satisfactory correlation between the experimental and numerical temperatures is achieved by the R–ALE model in the case of an unlubrificated drilling operation. After rebuilding the Lagrangian thermal history of the final workpiece, the thermal residual stresses can be computed by means of a standard thermo-elastoplastic simulation. The first results are interesting, but the mechanical loadings due to drilling will be considered in a future study to improve the distribution of computed residual stresses.

Acknowledgements

The authors would like to thank Ugo Masciantonio and Fabien Lefebvre from CETIM, Erwan Jourden and Alexandre Brosse from AREVA NP, Christophe Claudin and Joel Rech from LTDS for the valuable discussions they had with them.

References

[1] C.H. Huang, L.C. Jan, R. Li, A.J. Shih, A three-dimensional inverse problem in estimating the applied heat flux of a titanium drilling – Theoretical and experimental studies, Int. J. Heat Mass Transf. 50 (2007) 3265–3277.
[2] P.F.B. De Sousa, V.L. Borges, I.C. Pereira, M.B. Da Silva, G. Guimarães, Estimation of heat flux and temperature field during drilling process using dynamic observers based on Green's function, Appl. Therm. Eng. 48 (2012) 144–154.
[3] V. Schulze, F. Zanger, J. Michna, F. Lang, 3D-FE-modelling of the drilling process – Prediction of phase transformations at the surface layer, Proc. CIRP 8 (2013) 33–38.
[4] J. Wu, R. Di Han, A new approach to predicting the maximum temperature in dry drilling based on a finite element model, Mater. Manuf. Process. 11 (1) (2009) 19–30.
[5] B. Ozcelik, E. Bagci, Experimental and numerical studies on the determination of twist drill temperature in dry drilling: a new approach, Mater. Des. 27 (2006) 920–927.
[6] X. Nan, L. Xie, W. Zhao, On the application of 3D finite element modeling for small-diameter hole drilling of AISI 1045 steel, Int. J. Adv. Manuf. Technol. (2015).
[7] M. Abouridouane, F. Klocke, D. Lung, O. Adams, Size effects in micro drilling ferritic-pearlitic carbon steels, Proc. CIRP 3 (2012) 91–96.
[8] M. Abouridouane, F. Klocke, D. Lung, Microstructure-based 3D finite element model for micro drilling carbon steels, Proc. CIRP 8 (2013) 94–99.
[9] M. Abouridouane, F. Klocke, D. Lung, O. Adams, A new 3D multiphase FE model for micro cutting ferritic-pearlitic carbon steels, CIRP Ann. 61 (1) (2012) 71–74.
[10] M. Abouridouane, F. Klocke, B. Döbbeler, Characterisation and modelling of the machinability of ferritic-pearlitic steels in drilling operations, Proc. CIRP 58 (2017) 79–84.
[11] T.D. Marusich, S. Usui, J. Ma, D.A. Stephenson, Finite Element Modeling of Drilling Processes with Solid and Indexable Tooling in Metals and Stack-ups, 2014.
[12] R. Muhammad, N. Ahmed, Y.M. Shariff, V.V. Silberschmidt, Effect of cutting conditions on temperature generated in drilling process: a FEA approach, Adv. Mater. Res. 223 (2011) 240–246.
[13] N. Ahmed Muhammad, Y.M. Shariff, V.V. Silberschmidt, Finite-element analysis of forces in drilling of Ti-alloys at elevated temperature, Solid State Phenom. 188 (2012) 250–255.
[14] F. Valiorgue, J. Rech, H. Hamdi, P. Gilles, J.M. Bergheau, A new approach for the modelling of residual stresses induced by turning of 316L, J. Mater. Process. Technol. 191 (1–3) (2007) 270–273.
[15] D.N. Arnold, F. Brezzi, M. Fortin, A stable element for the Stokes equations, Calcolo 21 (1984) 337–344.
[16] M. Girinon, F. Valiorgue, V. Robin, E. Feulvarch, 3D stationary simulation of a turning operation with an Eulerian approach, Appl. Therm. Eng. 76 (2015) 134–146.
[17] C. Claudin, Influence des conditions opératoires sur le procédé de perçage: Application aux structures mécano-soudées en acier bas carbone, PhD Thesis, ENSAM, 2006 (in French).
[18] E. Feulvarch, J.-C. Roux, J.-M. Bergheau, A simple and robust moving mesh technique for the finite element simulation of Friction Stir Welding, J. Comput. Appl. Math. 246 (2013) 269–277.
[19] ESI Group, User's manual, 2017.
[20] R. Zaera, J.A. Rodríguez-Martínez, D. Rittel, On the Taylor–Quinney coefficient in dynamically phase transforming materials. Application to 304 stainless steel, Int. J. Plast. 40 (2013) 185–201.

[21] O. Lurdos, F. Montheillet, G. Damamme, Empirical and physically based flow rules relevant to high speed processing of 304L steel, Int. J. Mater. Form 1 (Suppl. 1) (2008) 1431–1434.
[22] M. Girinon, F. Dumont, F. Valiorgue, J. Rech, E. Feulvarch, F. Lefebvre, H. Karaouni, E. Jourden, Influence of lubrication modes on residual stresses generation in drilling of 316L, 15-5PH and Inconel 718 alloys, https://doi.org/10.1016/j.procir.2018.05.020.
[23] E. Feulvarch, M. Fontaine, J.-M. Bergheau, XFEM investigation of a crack path in residual stresses resulting from quenching, Finite Elem. Anal. Des. 75 (2013) 62–70.
[24] P.J. Armstrong, C.O. Frederick, A Mathematical Representation of the Multiaxial Bauschinger Effect, CEGB Report No. RD/B/N 731, 1966.